Lithium–Niobium–Titanium–Oxide Ceramics with ZnO as a Functional Additive: Structural and Impedance Characterization with Humidity Properties

R.R. Raonić[a], D.L. Sekulić[b], S.R. Lukić-Petrović[a] and T.B. Ivetić[a,*]

[a] *University of Novi Sad, Faculty of Sciences, Department of Physics, Trg Dositeja Obradovića 3, 21000 Novi Sad, Serbia*
[b] *University of Novi Sad, Faculty of Technical Sciences, Department of Power, Electronic and Telecommunication Engineering, Trg Dositeja Obradovića 6, 21000 Novi Sad, Serbia*

Received: 25.02.2022 & Accepted: 30.08.2022

Doi: 10.12693/APhysPolA.142.457 *e-mail: tamara.ivetic@df.uns.ac.rs

For potential applications in electronic components and sensor elements, lithium–niobium–titanium oxide ceramics are prepared by a solid-state reaction method. Two different weight percentages (2 and 5 %) of ZnO as a functional additive are added before the mechanical milling step in two separate procedures and changes in microstructure, and electrical properties are investigated. Analysis of microstructure by scanning electron microscopy showed the morphology of the synthesized particles in the form of plates and rods, which corresponds to the desired microstructure of the M-phase class of lithium–niobium–titanium oxide ceramic materials. The addition of ZnO creates a trend of increasing the total bulk density. X-ray diffraction analysis by Rietveld refinement and deconvolution of the Raman spectra by Lorentzian line shape fitting enabled the characterization of the crystal structure and vibration properties. In the frequency range from 100 Hz to 10 MHz, the analysis of the obtained impedance spectra at room temperature shows that the tested samples have non-Debye dielectric relaxation. Furthermore, the appearance of one semicircle on the Cole–Cole plots indicates the dominant influence of grain boundary effects on the electrical behavior of the studied ceramics in the measurement frequency range. Finally, a room temperature study of the humidity sensing properties showed that the 2% ZnO sample had a better linear impedance change response over a wide range of relative humidity from 15% to 85% at a frequency of 15 kHz.

topics: ceramics, microstructure, impedance, humidity sensing

1. Introduction

Lithium–niobium–titanium oxide (LNTO) ceramics, especially their so-called M-phase class of compounds with the general formula $Li_{1+x-y}Nb_{1-x-3y}Ti_{x+4y}O_3$ ($0.05 < x < 0.3$, $0 < y < 0.182$) that was first reported by Villafuerte-Castrejón et al. [1], show excellent microwave dielectric properties [2–4]. This makes them a very desirable material for use in microwave electronic components such as resonators and waveguides, as well as in microelectronics in general. Also, recent studies show its favorable thermistor characteristics suitable for potential applications in sensors [5]. However, the higher sintering temperature, which is usually above 1100°C [6–10] for the production of LNTO materials, sets a new goal of lowering it for more economical production, but also to meet the requirements for use with Ag, Ag/Pd, or Au electrode materials in low temperature co-fired ceramic (LTCC) technology [11]. In this regard, several different methods have been used that allow the application of lower synthesis temperature, such as sol–gel methods and molten salt methods [2, 12, 13], but the most promising is the use of additives of low melting point compounds (B_2O_3, MoO_3, Bi_2O_3) [14–18] in the conventional solid reaction method. The conventional method of ceramic production begins with the mechanical grinding of oxide precursors to increase the chemical reactivity of the starting components or for simple physical homogenization required to control morphology, texture, and particle size distribution [19, 20] and ends with sintering heat treatment. The addition of ZnO to the synthesis mixture before the grinding step can have several effects on ceramics in terms of their properties and potential application [21]. One of the typical effects of ZnO addition is a decrease in the sintering temperature (as well as the glass transition temperature and crystallization temperature in glass-ceramics [22]). ZnO also improves the density and dielectric properties of ceramics [23]. Density is closely related to other

mechanical properties, such as porosity and grain size, all of which are important factors for sensors and electronic applications. The addition of ZnO increases the hardness and fracture toughness and improves ferroelectricity [24–26]. In general, the optical, electrical, and dielectric properties of ceramics can be significantly altered by the addition of ZnO as it reduces the optical band gap and contributes to the much desired high dielectric constant and low tangent loss [27].

Aiming to provide valuable information both from the point of view of fundamental scientific interest and from the point of view of their potential application to various microelectronic devices, this study investigates the effect of ZnO addition on the electrical and microstructural properties of *M*-phase type lithium–niobium–titanium oxide ceramics. In one of the important applications, humidity sensors based on ceramic materials can detect humidity on the principle of changing the electrical properties of the sensing material by adsorption of water vapor and their penetration through the open pores of the sensing material, which results in significant changes in their electrical characteristics [28]. For this purpose, the impedance of the prepared LTNO ceramics was measured as a function of relative humidity (RH) at different frequencies and room temperature.

2. Experimental work

2.1. Materials synthesis

The lithium–niobium–titanium oxide (LNTO) ceramic samples were prepared by a solid-state procedure consisting of wet-milling in ethanol and sintering. Powder precursors for the synthesis of LNTO, TiO_2 anatase (99.7%, $<$ 25 nm particle size, Aldrich Chemistry), Nb_2O_5 (99.9%, Alfa Aesar), and Li_2CO_3 (Kemika, Zagreb), were first mixed in the desired $Li_7Nb_3Ti_5O_{21}$ stoichiometry. The 2 wt% ZnO (99.999%, Aldrich Chemistry) was added as a functional additive to the first sample powders mixture before the milling step (hereinafter 2% ZnO), and 5 wt% of ZnO was added to the second sample powder mixture (hereinafter 5% ZnO). The powder mixtures were wet-milled in ethanol in two separate procedures for 4 hours with a ball mill (Retsch PM100) using a zirconia vial and 5 mm in diameter zirconia balls. The ball to powder mass ratio was 10:1, and the rotation speed was 100 rpm. Thereafter, the powder mixtures were air-dried for about 24 h and calcinated in a furnace at 650°C for 4 h using alumina crucibles to dispose of the organic components. The next processing step was to form the pellets from the milled powders using a 10 mm diameter mold and a Specac hydraulic press with a uniaxial pressure of about 784 MPa. Finally, the resulting pellets were sintered at 900°C for 4 h. An illustrative diagram of the described procedure is shown in Fig. 1.

2.2. Materials characterization

The bulk density of sintered LNTO was determined by the pycnometric method. X-ray diffraction (XRD) was performed using a Rigaku MiniFlex 600 diffractometer with Cu $K_{\alpha 1/2}$ radiation and a step scan mode of 0.02° /3 s in the angular range 2θ = 10-70° . The resulting XRD patterns were analyzed by the Rietveld method of structure refinement using the FullProf Suite [29]. Scanning electron microscopy (SEM) was performed on a JEOL JSM-6460LV. Raman spectra were obtained using a confocal DXR Raman microscope (Thermo Fisher Scientific Inc., USA), equipped with a diode-pumped solid-state (DPSS) green laser (wavelength 532 nm) with a maximum laser power level of 24 mW. The laser used for excitation is connected to an Olympus optical microscope and a 10 magnification objective, which focuses the laser beam onto the sample. All data were plotted and analyzed using OMNIC software.

The measurement of complex impedance spectroscopy (IS) was performed on the obtained sintered pellets, which were first polished and then coated on both sides with silver paste. The electrical parameters, parallel resistance (R_p) and parallel capacitance (C_p), were obtained over a wide frequency range (100 Hz–10 MHz) at room temperature using a computer-controlled impedance analyzer HP 4194A. The experimental setup included a RIIC VLT−2 chamber to ensure normal ambient conditions, as well as sample heating using a Beckman CTC 250 temperature controller with an accuracy of ±0.5°C. Experimentally measured parallel values of resistance and capacitance were converted and presented in the form of complex impedance

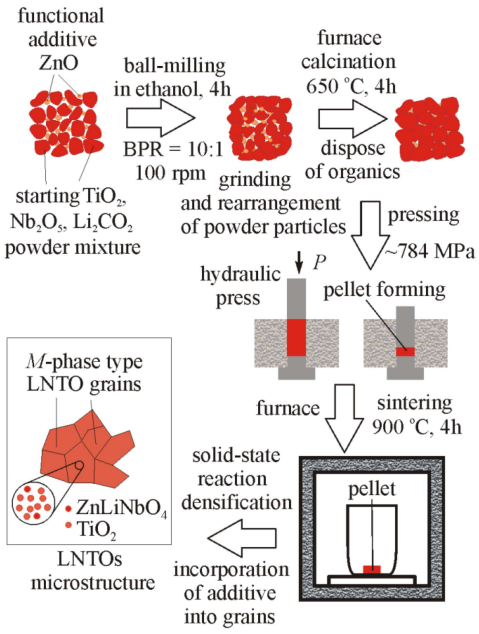

Fig. 1. Illustration of the solid-state *M*-phase LNTO synthesis.

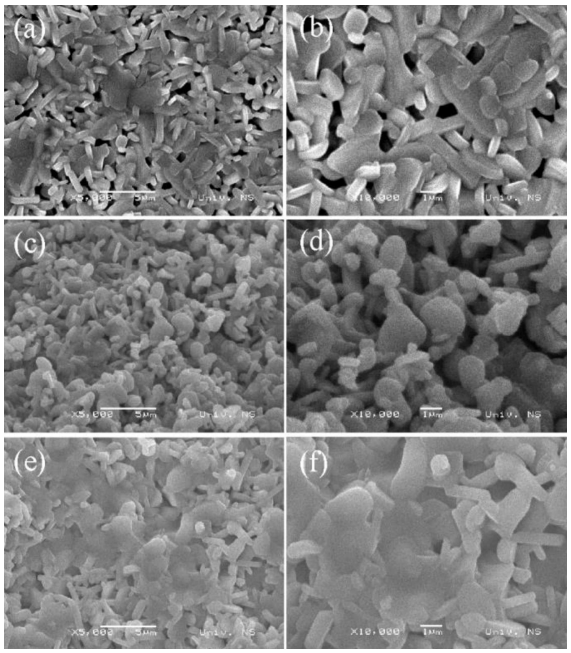

Fig. 2. SEM images at two different magnifications (×5,000 and ×10,000) of (a), (b) unmodified LNTO, (c), (d) 2% ZnO, and (e), (f) 5% ZnO samples.

as previously described [30, 31]. Impedance data fitting analysis was performed using EIS Spectrum Analyzer software [32] with about 2% fitting errors.

To study the humidity sensing performance, the prepared ceramic pellets were placed as sensing elements in a closed test glass chamber between two silver electrodes, which are connected to a computer-controlled impedance analyzer HP 4194A to measure the change in impedance with respect to relative humidity at 25 ± 0.5°C. The compressed air directed into the chamber was first dehydrated over silica gel and $CaCl_2$, and then the humidity level was varied from 15 to 85% by passing the air through water and mixing it with dry air. In such a measurement system, RH and temperature are monitored using a commercial humidity and temperature probe (Tecpel DTM-321) [33].

3. Results and discussion

3.1. Microstructure characterization

SEM images of unmodified LNTO, 2% ZnO, and 5% ZnO samples are shown in Fig. 2. Rod-shaped and plate-shaped particles, which are morphological characteristics of the M-phase, were observed. The bulk density of the sample 5% ZnO ($\rho_{5\%}$ = 3.98 g/cm^3) is higher than the bulk density of the sample 2% ZnO ($\rho_{2\%}$ = 3.88 g/cm^3) and even higher than the bulk density of unmodified LNTO ceramics ($\rho_{0\%}$ = 3.60 g/cm^3) prepared in the same way but without ZnO additive. LNTO ceramics

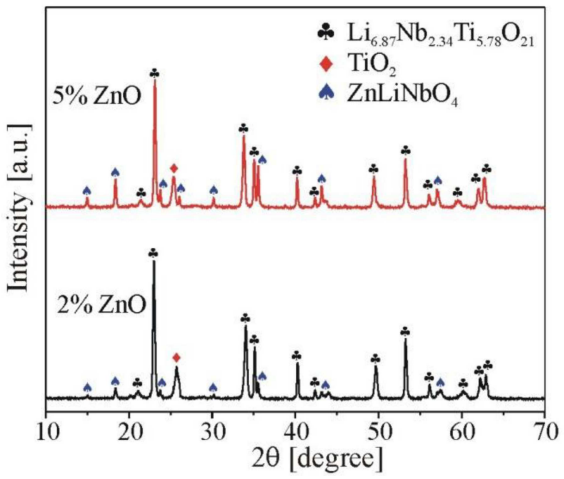

Fig. 3. XRD patterns of 2% ZnO and 5% ZnO samples.

TABLE I

Structural parameters of $Li_{6.87}Nb_{2.34}Ti_{5.78}O_{21}$ calculated by Rietveld refinement. Here, R is R-factor, the statistical parameter of quality.

Sample	2% ZnO	5% ZnO
Crystallite size [nm]	163.7	–
Strain [%]	29.68	–
a [Å]	5.1288	5.0420
b [Å]	5.1288	5.0420
c [Å]	32.8462	33.5435
R	24.7	39.2

become less porous with the addition of ZnO (Fig. 2) due to easier diffusion supported by the ZnO oxygen loss starting from 850°C when Frenkel defects, a new phase, and grain growth appears. Similar behavior was observed for the M-phase LNTO ceramics modified with B_2O_3 [14, 15], which showed an increase in density at sintering temperatures even below 900°C compared to unmodified LNTO ceramics sintered at ∼ 1000°C whose bulk density was approx. 3.28 g/cm^3 [34].

3.2. XRD and Raman structural analysis

The main phase is indexed as $Li_{6.87}Nb_{2.34}Ti_{5.78}O_{21}$ structure (COD reference card no. 1533457) belonging to $P\bar{3}c1$ no. 165 space group of the trigonal crystal system. Traces of the initial TiO_2 anatase (JCPDS cards no. 21-1272) and the new phase $ZnLiNbO_4$ (JCPDS cards no. 23-1206) appear in the XRD patterns (Fig. 3). With the increase of ZnO additive, a certain increase in the XRD intensity of $ZnLiNbO_4$ peaks was observed. A better Rietveld refinement of the structure was achieved for 2% ZnO, where the average crystallite size of about 164 nm was calculated for the $Li_{6.87}Nb_{2.34}Ti_{5.78}O_{21}$ phase,

TABLE II

Raman peaks frequency [cm^{-1}], intensity, and full width at half maximum (FWHM) from simultaneous peak fits to Lorentzian line shape, reference values, and proposed symmetry mode assignments.

Sample No.	2% ZnO			5% ZnO			Refs. [34–37]	
	Peak position [cm-^{1}]	Intensity	FWHM	Peak position [cm^{-1}]	Intensity	FWHM	Peak position [cm^{-1}]	Mode assignment
1	71	0.29	14.1	56	0.23	7.9		
2	99	0.11	33	103	0.30	33.3	99	Zn–O motions
3	150	0.32	16.5	150	0.62	16.2	151	Nb–O motions
4	245	0.44	42.6	246	0.88	39.3	240	O–Ti–O bending
5	279	0.71	21.4	279	0.56	21.3	278	Li displacements
6	363	0.54	34.2	356	0.53	31.3	358	Li displacements
7	405	0.41	53	409	0.88	84.3	410	Zn-O motions
8	442	0.23	38				430	O–Nb–O bending coupled with Li–O and O–Li–O bending modes, or Li–O stretching in LiO_6
9	587	0.49	145.6	579	0.71	98	585	O–Nb–O stretching
				660	0.32	112	666	Zn–O motions
10	752	0.12	36	750	0.15	55	753	Ti–O motions in TiO_6
11	883	0.37	30.0	881	0.58	30.6	881	O motions in NbO_6

while for the 5% ZnO sample, only the values for lattice parameters could be calculated. The obtained results of Rietveld refinement are presented in Table I.

According to XRD and SEM results, ZnO plays a role in promoting densification of LNTO (Fig. 2) mainly in the initial and middle stages of sintering [35], since ZnO was found to be incorporated into LNTO ceramic grains as the $ZnLiNbO_4$ phase (Fig. 3).

The fitting of the Raman spectra was performed using the line shape of the Lorentzian function (Fig. 4). Vibration modes were assigned by comparison with the Raman spectrum of LNTO described in our recent publication [5] (see Table II), but also by taking into account the vibrational motions of Zn–O in $ZnLiNbO_4$ [36–38]. Significant differences were observed mainly as an increase in the intensity (Table II) of some vibration modes and the appearance of another peak at 660 cm^{-1}, which is probably related to Zn–O motion because it occurs when the weight percentage of functional ZnO additive is increased.

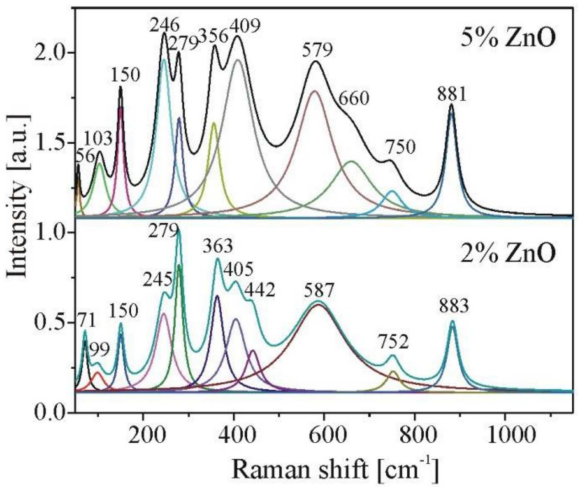

Fig. 4. Deconvolution of the Raman spectra of the 2% ZnO and 5% ZnO samples.

3.3. Impedance spectroscopy

As a widely used, powerful, and non-destructive technique for the characterization of polycrystalline electroceramic materials, impedance spectroscopy was applied in this study to analyze electrical processes occurring within the synthesized LNTO samples. Impedance spectra in a wide frequency range from 100 Hz to 10 MHz were measured at room temperature, and the obtained results are shown in Fig. 5. It is noted that both Cole–Cole plots for LNTO with 2 wt% and 5 wt% ZnO additives are characterized by the presence of only one incomplete semicircle, even though it is common for these plots to have two semicircles showing the contribution of grains and grain boundaries, which are the two main components of the microstructure of ceramic materials. This behavior indicates that the grain boundary has a dominant effect on the conduction mechanism and that the grain contribution cannot be determined for both LNTO samples within the measurement frequency range. This may be due to the limited frequency range used in this study (100 Hz–10 MHz) or the impedance

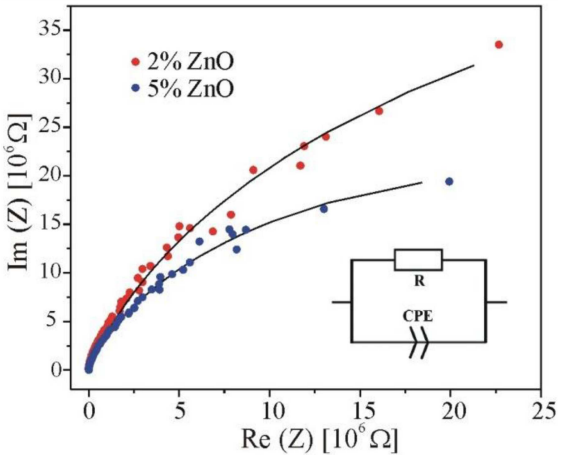

Fig. 5. Impedance spectra of 2% ZnO and 5% ZnO samples at room temperature. Lines are fitted curves obtained using the equivalent circuit model, which is shown as an inset.

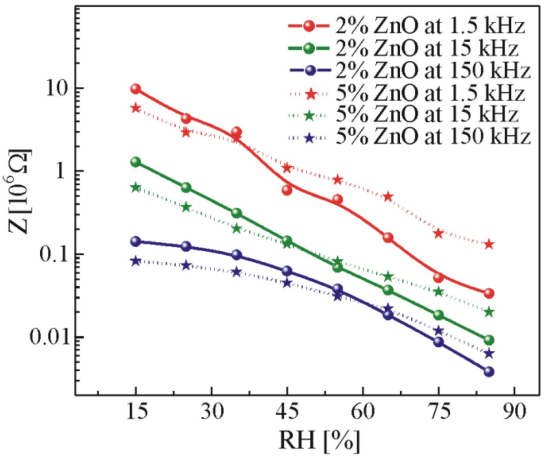

Fig. 6. Dependence of the impedance of LTNO ceramics with 2 wt% and 5 wt% ZnO to relative humidity at different frequencies and room temperature.

TABLE III

Determined values of electrical circuit model parameters from impedance analysis.

Sample	2% ZnO	5% ZnO
R	1.0157×10^8 Ω	5.1026×10^7 Ω
CPE	5.3009×10^{-11} F	9.7131×10^{-11} F
n	0.858	0.855
T	2.269 ms	2.015 ms

response of grains and grain boundaries overlapping, preventing separation of boundary contribution from the grain contribution by impedance spectroscopy [5, 39, 40].

Moreover, the obtained impedance data show that the centers of the semicircles lie below the real axis of the impedance, which is a prominent feature of the non-Debye type relaxation mechanism [31]. In addition, it is evident from the Cole–Cole plot that the semicircle radius for LNTO with 2 wt% ZnO addition is larger than that for LNTO with 5 wt% ZnO additive, indicating that the resistance of the LTNO material is reduced by ZnO addition. For a more detailed analysis of the impedance response for LTNO, the resulting Cole–Cole plots are modeled using an equivalent electrical circuit based on only one parallel R–CPE element, as shown in the inset in Fig. 5. In this model, R and CPE represent, respectively, the resistance and the constant phase element for the grain boundaries, which should account for the observed non-ideal Debye behavior of both LTNO samples in this study. In the proposed model, these parameters were determined by fitting a Cole–Cole plot with 0.2–3.4% fitting errors using the free software EIS Spectrum Analyzer. The determined parameter values are summarized in Table III and follow our previous results on LNTO with $<$ 1 wt% of ZnO additive [5].

The validity of the proposed electrical circuit is confirmed by the close agreement of the experimentally obtained Cole–Cole plots (scattered) and the curves obtained by fitting (lines), as can be seen in Fig. 5. Furthermore, impedance analysis showed that LNTO with 2 wt% ZnO additive has higher resistance and lower grain boundary capacitance compared to LNTO with 5 wt% ZnO additive, as can be seen in Table III. The values of equivalent circuit model parameters show that the grain boundary relaxation time ($\tau = (R \times CPE)^{1/n}$) for both samples is approximately the same value. In addition, the calculated value of the parameter n for both LTNO samples is about 0.86, which indicates non-ideal behavior since this value is sufficiently less than 1 [41].

To study the humidity sensing performance, the impedance Z of the as-prepared LTNO ceramics was measured as a function of RH at different frequencies and room temperature. The obtained results for several frequencies in the RH range between 15% and 85% are shown in Fig. 6. It is obvious that the impedance of samples with 2% ZnO and 5% ZnO is significantly affected by RH and decreases with increasing RH. This observed effect is more pronounced in the synthesized LTNO ceramics with a lower weight percentage of ZnO, which is consistent with the fact that this sample has a higher porosity. The high sensitivity to humidity and linear response in the entire RH range were observed at relatively low measurement frequency, i.e., at 15 kHz. At this frequency, the impedance changes by about two orders of magnitude as RH increases. This significant decrease in impedance values with RH can be attributed to the adsorption of water molecules [42, 43]. However, at a higher measurement frequency (i.e., 150 kHz), the impedance plots become flat because the direction of the applied electric field changes faster and

the polarization of the adsorbed water molecules cannot catch up [33, 44]. Therefore, a frequency of 15 kHz was chosen as the optimal operating frequency of the sensor based on LTNO ceramics with 2 wt% ZnO.

4. Conclusions

This paper reports changes in structure, morphology, and electrical properties with an increasing weight percentage of ZnO as a functional additive for the M-phase type lithium–niobium–titanium–oxide ceramics synthesized in the solid-state, which is a very promising material for applications in microelectronics and sensor. The successful formation of the characteristic M-phase microstructure has been repeatedly confirmed using several experimental techniques (XRD, Raman, and SEM). The dominant role of grain boundaries in the conduction mechanism was confirmed by the obtained measurement results and the analysis of the impedance response. Furthermore, the results show that LTNO ceramics with a low weight percentage of ZnO can be proposed as a promising material for humidity sensing devices.

Acknowledgments

This research is financed by the Ministry of Education, Science and Technological Development of the Republic of Serbia (grants number 451-03-68/2022-14/200125 and 451-03-9/2021-14/200156, and project DS 13, APVV DS-FR-19-0036), and partially financed by the APV Provincial Secretariat for Higher Education and Scientific Research (Project title: "Development of new highly-sensitive sensors for monitoring of gas pollution and humidity in Vojvodina" project no. 142-451-2635/2021-01/2). The authors thank Srđan Rakić for XRD, Elvira Tóth for Raman measurements, and Radenko Kisić for technical assistance from the Department of Physics, Faculty of Sciences, University of Novi Sad, Serbia.

References

[1] M.E. Villafuerte-Castrejón, A. Aragón-Pina, R. Valenzuela, A.R. West, *J. Solid State Chem.* **71**, 103 (1987).

[2] Y. Long, Y. Li, Y. Wang, W. Wu, *J. Alloys Compd.* **475**, 546 (2009).

[3] S. Xu, J. Jiang, Z. Cheng, X. Chen, S. Sun, D. Wang, T. Zhang, *Crystals* **11**, 741 (2021).

[4] Q. Zeng, W. Li, J.L. Shi, J.K. Guo, *Mater. Lett.* **60**, 3203 (2006).

[5] T.B. Ivetić, Y. Xia, O. Benzine, J. Petrović, J. Papan, S.R. Lukić-Petrović, A.P. Litvinchuk, *Ceram. Int.* **47**, 4944 (2021).

[6] A.Y. Borisevich, S.V. Kalinin, D.A. Bonnell, P.K. Davis, *J. Mater. Res.* **16**, 329 (2001).

[7] A.Y. Borisevich, P.K. Davies, *J. Am. Ceram. Soc.* **85**, 573 (2002).

[8] Q. Zeng, W. Li, J. Shi, X. Dong, J. Guo, *J. Am. Ceram. Soc.* **91**, 644 (2008).

[9] I.E. Gray, P. Bordet, C. Li, R.S. Roth, *J. Solid State Chem.* **177**, 660 (2004).

[10] Z. Liu, Y. Wang, W. Wu, Y. Li, *J. Asian Ceram. Soc.* **1**, 2 (2013).

[11] H. Yu, J. Liu, W. Zhang, S. Zhang, *J. Mater. Sci. Mater. Electron.* **26**, 9414 (2015).

[12] X. Wang, W. Li, J. Shi, *Particuology* **8**, 463 (2010).

[13] Z. Lu, Y. Wang, W. Wu, Y. Li, *J. Alloy. Compd.* **509**, 9696 (2011).

[14] Q. Zeng, Y. Zhou, L. Huo, *Mater. Chem. Phys.* **129**, 892 (2011).

[15] Q. Zeng, W. Li, J. Shi, J. Guo, H. Chen, M. Liu, *J. Eur. Ceram. Soc.* **27**, 261 (2007).

[16] D. Zhou, C.A. Randall, H. Wang, L. Pang, X. Yao, *J. Am. Ceram. Soc.* **93**, 1096 (2010).

[17] T. Ivetić, M.V. Nikolić, M. Slankamenac, M. Živanov, D. Minić, P.M. Nikolić, M.M. Ristić, *Sci. Sinter.* **39**, 229 (2007).

[18] M. Slankamenac, T. Ivetić, M.V. Nikolić, N. Ivetić, M. Živanov, V.B. Pavlović, *J. Electon. Mater.* **39**, 447 (2010).

[19] T. Ivetić, Z. Vuković, M.V. Nikolić, V.B. Pavlović, J.R. Nikolić, D. Minić, M.M. Ristić, *Ceram. Int.* **34**, 639 (2008).

[20] Lj.R. Đačanin, M.D. Dramićanin, S.R. Lukić-Petrović, D.M. Petrović, M.G. Nikolić, T.B. Ivetić, I.O. Gúth, *Ceram. Int.* **40**, 8281 (2014).

[21] H. Zhou, H. Wang, D. Zhou, L. Pang, X. Yao, *Mater. Chem. Phys.* **109**, 510 (2008).

[22] G. Chen, *J. Mater. Sci. Mater. Electron.* **18**, 1253 (2007).

[23] X. Ji, F. Yi, S. Zhang, C. Zhai, P.Hu, *Key Eng. Mater.* **616**, 145 (2014).

[24] M. Promsawat, A. Watcharapasorn, S. Jiansirisomboon, *Nanoscale Res. Lett.* **7**, 65 (2012).

[25] M. Promsawat, A. Watcharapasorn, T. Sreesattabud, S. Jiansirisomboon, *Ferroelectrics* **382**, 1 (2009).

[26] M. Promsawat, A. Watcharapasorn, S. Jiansirisomboon, *Ceram. Int.* **38**, S215 (2012).

[27] Y. Slimani, A. Selmi, E. Hannachi, M.A. Almessiere, A. Bayka, I. Ercan, *J. Mater. Sci. Mater. Electron.* **30**, 9520 (2019).

[28] T.A. Blank, L.P. Eksperiandova, K.N. Belikov, *Sensor. Actuat. B Chem.* **228**, 416 (2016).

[29] J. Rodriguez-Carvajal, *Physica B. Condensed Matter.* **192**, 55 (1993).

[30] M.V. Nikolic, M.P. Slankamenac, N. Nikolic, D.L. Sekulic, O.S. Aleksic, M. Mitric, T. Ivetic, V.B. Pavlovic, P.M. Nikolic, *Sci. Sinter.* **44**, 307 (2012).

[31] T.B. Ivetić, D.L. Sekulić, J. Papan, I.O. Gúth, D.M. Petrović, S.R. Lukić-Petrović, *Ceram. Int.* **44**, 18987 (2018).

[32] A.S. Bondarenko, G.A. Ragoisha, in: *Progress in Chemometrics Research*, Ed. A.L. Pomerantsev, Nova Science Publishers, New York 2005, p. 89.

[33] D.L. Sekulić, Z.Ž. Lazarević, N.Ž. Romčević, in: *31st Int. Conf. on Microelectronics (MIEL 2019)*, 2019, p. 95.

[34] Q. Zeng, W. Li, J.L. Shi, J.K. Guo, M.W. Zuo, W.J. Wu, *J. Am. Ceram. Soc.* **89**, 1733 (2006).

[35] N.C. Rosero-Navarro, T. Yamashita, A. Miura, M. Higuchi, K. Tadanaga, *J. Am. Ceram. Soc.* **100**, 276 (2017).

[36] B. Zhang, L. Li, W. Luo, *J. Alloy. Compd.* **771**, 15 (2019).

[37] R. Cuscó, E. Alarcón-Lladó, J. Ibáñez, L. Artús, *Phys. Rev. B* **75**, 165202 (2007).

[38] T.B. Ivetić, N.L. Finčur, B.F. Abramović, M. Dimitrievska, G.R. Štrbac, K.O. Čajko, B.B. Miljević, Lj.R. Đačanin, S.R. Lukić-Petrović, *Ceram. Int.* **42**, 3575 (2016).

[39] D.L. Sekulić, Z.Z. Lazarević, D. Jovalekić, A.N. Milutinović, N.Z. Romčević, *Sci. Sinter.* **48**, 17 (2016).

[40] M.V. Nikolić, D.L. Sekulić, Z.Z. Vasiljević, M.D. Luković, V.B. Pavlović, O.S. Aleksić, *J. Mater. Sci.-Mater. El.* **28**, 4796 (2017).

[41] K.O. Čajko, D.L. Sekulić, S. Lukić-Petrović, M.V. Šiljegović, D.M. Petrović, *J. Mater. Sci. Mater. Electron.* **28**, 120 (2017).

[42] V.R. Khadse, S. Thakur, K.R. Patil, P. Patil, *Sensor. Actuat. B Chem.* **203**, 229 (2014).

[43] D.L. Sekulić, Z.Ž. Lazarević, Č. Jovalekić, N.Ž. Romčević, in: *30th Int. Conf. on Microelectronics (MIEL 2017)*, 2017, p. 135.

[44] Z. Duan, M. Xu, T. Li, Y. Zhang, H. Zou, *Sensor. Actuat. B Chem.* **258**, 527 (2018).